Photocatalytic decolorization of cationic and anionic dyes over ZnO nanoparticle immobilized on natural Tunisian clay

Haithem Bel Hadjltaief, Sameh Ben Ameur, Patrick da Costa, Mourad Ben Zina, Maria Elena Galvez

Photocatalytic decolorization of cationic and anionic dyes over ZnO nanoparticle immobilized on natural Tunisian clay

Haithem Bel Hadjltaief [1], Sameh Ben Ameur[2], Patrick Da Costa[3], Mourad Ben Zina [1], Maria Elena Galvez [3]*

[1] Laboratory of « Eau, Energie et Environnement», National Engineering school of Sfax, University of Sfax, B.P1173.W.3038, Sfax, Tunisia

[2] Research Unit: Physics of insulators and semi insulator materials, Faculty of Science of Sfax, University of Sfax, Road of Soukra Km 3.5, B.P: 1171, 3038 Sfax, Tunisia

[3] Sorbonne University, UPMC, Univ. Paris 6, Institut Jean Le Rond d'Alembert, 2 place de la gare de ceinture, 78210 Saint-Cyr-L'Ecole, France

[*]*Corresponding author:* ***Sameh Ben Ameur and Haithem Bel Hadjltaief***

Email: sameh.benameur@yahoo.fr

Email: bel_hadj22@yahoo.com

Abstract

In the present work we describe a simple and low-cost method for the decolorization of textile dyeing and printing wastewaters, using ZnO as photocatalyst supported on natural Tunisian clay (ZnO/Clay). This composite ZnO/Clay material was synthesized through a sol–gel method. X-ray diffraction (XRD), Nitrogen Physisorption (BET), Infrared Spectroscopy (FTIR), Scanning Electronic Microscopy (SEM) and High-Resolution Transmission Electron Microscopy (HRTEM) linked with Energy Dispersive X-ray (EDX), were performed in order to explain the characteristics of the ZnO/Clay photocatalyst. The XRD patterns, pointing to the presence of ZnO of very small crystal sizes, i.e. highly dispersed on the clay surface. The photocatalytic activity of ZnO/Clay was assayed in the decolorization of a cationic dye (Malachite Green, MG) and anionic dyes (Red Congo, RC) in aqueous solution as models pollutants under UV irradiation. In addition, the effects of different parameters such as pH of the solution, catalyst dosage, concentration of the dyes, irradiation source, as well as the influence of the presence of inorganic ions were investigated. The ZnO/Clay photocatalyst exhibited high photocatalytic activity of MG and CR decolorization under simulated solar compared to UV irradiation. The recyclability of the ZnO/Clay photocatalyst was as well validated.

KEYWORDS: *Cationic and Anionic Dyes, Decolorization, Tunisian Clay, ZnO, Heterogeneous Photocatalyst.*

Introduction

Azo and triphenylmethane dyes, Malachite Green and Red Congo, are two of the most widely used colorants in various industries such as the textile, cosmetic, food, printing, paper and leather industries (Forgacs et al. 2004). Congo Red (CR), an anionic diazo dye, can be metabolized into benzidine, a well-known human carcinogen (Ong et al. 2016). Malachite Green (MG), a cationic triphenylmethane dye, is resistant to fading on exposure; when this dye is discharged into water it affects the aquatic life and can cause detrimental effects in the gills, intestine, liver, kidney and gonadotrophic cells (Bel Hadjltaief et al. 2013; Saikia et al. 2015). These pollutants are quite refractory to both aerobic and anaerobic digestions, and stable to light, heat, and moderate oxidizing agents, being thus difficult to remove (Bel Hadjltaief et al. 2013; Saikia et al. 2015). Therefore, the elimination of these pollutants from wastewater remains a very challenging task.

A wide range of methods have been developed aiming to the removal of Malachite Green and Red Congo dyes from the wastewaters such as adsorption, membrane separation, ion exchange, photocatalytic degradation and biological treatments (Bel Hadjltaief et al. 2013). Among these methods, semiconductor photocatalytic processes, show important removal efficiencies and have an important potential for industrial application. Photocatalytic proceses moreover allow full water decontamination under relative mild operation conditions (Bel Hadjltaief et al. 2014b).

Zinc oxide as a semiconductor, (ZnO, 3.37 eV), has been historically used for the removal of CR or MG from water due to its high photo sensitivity, large band-gap, stability and relatively low toxicity (Saikia et al. 2015; Balcha et al. 2016; Ong et al. 2016). Aiming to its practical utilization, ZnO has been immobilized on various supports such as zeolites (Nezamzadeh-Ejhieh

et al. 2014), activated carbon (Muthirulan et al. 2013; Soltani et al. 2014) and clay (Fatimah et al. 2011; Motshekga et al. 2013; Li et al. 2014; Ye et al. 2015; Zhou et al. 2015; Xu et al. 2015).

In particular, clay-based catalysts, i.e. metal oxide supported clays, have been frequently used in heterogenous photocatalytic applications (Bel Hadjltaief et al. 2014b; Bel Hadjltaief et al. 2016). These catalysts have been employed in the photocatalytic degradation of organic pollutants such as phenol and of some phenolic derivates (Zhou et al. 2015; Ye et al. 2015), organic dyes (Motshekga et al. 2013; Li et al 2014; Xu et al. 2014; Xu et al. 2015) and other persistent compounds (Dhakshinamoorthy et al. 2011; Abedi et al. 2015). For example, Xu and co-workers reported the preparation of a composite material consisting in ZnO loaded onto the surface of commercial Bentonite following an in situ sol–gel technique. Compared with the original raw clay and pure ZnO, the composite material exhibited considerably higher photocatalytic activity in the photodecomposition of Acid Red 35 in water solution under ultraviolet irradiation (Xu et al. 2015). In another study, ZnO particle supported on commercial Rectorite (ZnO/rectorite) was prepared through sol-gel synthesis using zinc acetate and lithium hydroxide as raw materials and Rectorite as support (Li et al. 2014). The photo-catalytic performance of such ZnO/rectorite was investigated in the removal of Methylene Blue under simulated solar irradiation. So far, to the best of our knowledge and according to the literature research, using ZnO supported on natural Tunisian clays has never been considered and used as a photocatalyst in the decolorization of organic dye-containing waters, under solar and UV irradiation.

In the present work, natural Tunisian clay was therefore used as a support for the immobilization of ZnO following a sol-gel method. The photocatalytic activity of this clay-supported ZnO was assayed in the decolorization of water containing both cationinc (Malachite

Green, MG) and anionic dyes (Red Congo, RC). The influence of key operational parameters, such as pH, catalyst dosage, initial dye concentration, has been considered. In addition, the potential interference of inorganic ions such as NO_3^-, SO_4^{2-}, HCO_3^- and Cl^- on the photocatalytic performance of ZnO/clay was also investigated.

Experimental

Materials and chemicals

The natural red clay (NC) used in this study was sampled in Jebel Tejera-Esghira deposits located in the Southeast of Tunisia from the area of Medenine (Bel Hadjltaief et al. 2017). From geological point of view, those clays were attributed to the Lower Triassic. It is a very thick series with dominant of sandstone alternating with red clays and with some silty intercalations. The outcrops extended from the Beni Kheddache cliff to the J. Tebaga of Medenine; it occupies the anticline of the J. Tajera site. The outcropping feature of the Jebel Tajera-Esghira was estimated to 80m-thick deposits of ferruginous clays (Bel Hadjltaief et al. 2017). The procedures used for its purification and Na-ion exchange from its surface have been previously described elsewhere (Bel Hadjltaief et al. 2014a; Bel Hadjltaief et al. 2016).

Zinc acetate dehydrate (zinc nitrate ($Zn(NO_3)_2$), 98%, Sigma–Aldrich, purity: 97%) was used as ZnO source for the preparation of the photocatalyst. Commercial ZnO (Merck, BET: 10 $m^2\ g^{-1}$) was used as a basis for comparison with our synthesized ZnO/Clay photocatalyst. Sodium chloride (NaCl), sodium sulfate (Na_2SO_4), sodium bicarbonate ($NaHCO_3$) and sodium nitrate ($NaNO_3$) were provided by Merck Chemical Company. All the chemicals were used as received without further treatment. Red Congo (RC) and Malachite Green (MG) dyes were used;

111 both supplied by Sigma Aldrich. The absorption peaks at 618 and 499 nm were used to monitor
112 the discoloration of MG and RC, respectively.

113 ***Synthesis of photocatalyst***

114 The ZnO/Clay was synthesized via an optimized sol–gel method (Abedi et al. 2015). To do so,
115 4.38 g of dehydratedzinc acetate were dissolved in 100 mL of ethanol and stirred in a water bath
116 at 50°C. Then, 2.98 g of tri-ethanolamine were subsequently added to the solution while stirring
117 continuously stirring for 1 h. The mixture was then placed under vibration and heated for 0.5 h at
118 40 °C, resulting in a colorless and transparent sol. At this instant, 3 g of natural clay were added
119 to this sol. The dispersion was further agitated under vibration for another 0.5 h, filtered, dried
120 and calcined for 4 h at 400 °C.

121 ***Raw clay and photocatalysts physico-chemical characterization***

122 Several techniques were employed for the characterization of both the natural clay and ZnO/Clay
123 catalyst. The identification of the different phases and crystal structures contained in the
124 ZnO/Clay catalysts was performed through XRD analysis. An X-ray diffractometer (Philips PW
125 1710, Japan) was used with CuKα (λ = 1.54056 Å) radiation over a range of 2θ angles from 10 to
126 70, with a step size of 0.02°/s. The Scherrer equation was applied for estimation of the crystal
127 size of ZnO on clay based catalyst.

128 Nitrogen adsorption–desorption isotherms for the different materials were acquired at − 196 °C
129 on a Micromeritics ASAP 2010, after outgassing (10^{-5} Pa) for 24 h at ambient temperature.
130 Surface areas were calculated using the BET equation, whereas mean pore size, pore size
131 distribution and pore volume were estimated using the BJH method (Bel Hadjltaief et al. 2016).

The surface functional groups were studied using Fourier transform infrared (FT-IR) spectroscopy (IR, Digilab Excalibur FTS 3000 spectrometer). 1 mg of the clay fraction (>2µm) was diluted in 200 mg KBr to quantify the superficial reactive sites.

The morphology of the natural and ZnO supported clay was studied using scanning electronic microscopy (SEM, Hitachi SU-70) and High Resolution Transmission Electron Microscopy (HRTEM, JEOL JEM 2011) coupled by EDX microanalyzer (PGT IMIX PC) to evaluate the chemical composition.

The zero point charge (pH_{ZPC}) of the prepared material was determined following the method described by Bouzid et al. (2008).

Photocatalytic activity and irradiation experiments

Photocatalytic discoloration experiments were performed in an open Pyrex-glass cell with 250 mL capacity (of 5cminside diameter and 11 cm height). A detailed description of photocatalytic reactor was reported in an earlier study (Bel Hadjltaief et al. 2013; Bel Hadjltaief et al. 2016). Irradiation was carried out using an UV-lamp (Black-Ray B 100WUV-lamp, V-100AP series) with a wavelength of 365 nm. The experiments under natural solar radiation were carried out during the month of September 2016 during sunny days in our laboratory Sfax (Tunisia) in front of the Chemistry Department without any obstacle and were started at 11:00 am for a total duration of 2 h.

For the discoloration of MG or RC under UV irradiation, 150 mg of ZnO /clay was added to 100 mL of each dye aqueous solutions (50 mg L^{-1}) at room temperature. The resulting suspension was first magnetically stirred for 60 min in the dark, in order to reach adsorption-desorption equilibrium. At specific time intervals 2–3 mL of sample was withdrawn and catalyst was

filtered using PTFE filters (0.45 μm). Concentration of MG and RC was then measured by means of UV–vis spectrophotometer (Shimadzu UV-vis spectrophotometer model 160A (Kyoto, Japan)), at the maximal adsorption wavelengths of RC and MG, λ_{max} = 497 nm and λ_{max} = 617 nm, respectively. Therefore, the dye discoloration efficiency was calculated as follows:

$$\text{Discoloration efficiency}\ (\%) = \left(1 - \frac{A_t}{A_0}\right) \times 100 \quad (1)$$

where A_0 represents the initial absorbance of the RC or MG solution, and A_t its absorbance after t minutes of irradiation/reaction.

The experimental work of this study involved several parameters on discoloration of the RC and MG dyes was studied. Firstly, the influence of the dye solution pH was assayed. The solution pH was adjusted from 2 to 12 using HCl (0.1 M) and NaOH (0.1 M), while fixing the dye concentration at 50 mg/L for either RC or MG and of the ZnO/clay catalyst at 1 g/L. The influence of the catalyst dosage, the ZnO/clay concentration was varied from 0.1 to 2 g/L, for 50 mg/L of either a RC or MG solution, at pH 8 for MG and pH 3 for RC. To assess the influence of the initial dye concentration, experiments were performed at either RC or MG concentrations of 100, 75, 50, 25, and 12.5 mg/L, respectively, while fixing the pH 8 for MG and pH 3 for RC, and ZnO/clay at 1 g/L. The potential interference of inorganic ions such as SO_4^{2-}, NO_3^-, CO_3^- and Cl^- on the photocatalytic performance of the ZnO/clay was also examined. The inorganic ions were added as sodium salts at the concentration of 1×10^{-3} mol/L. Finally, the stability of the ZnO/clay photocatalyst was evaluated in five consecutive experiments by using fresh RC or MG solutions at optimum condition pH 8 for MG and pH 3 for RC, 0.8 g/L catalyst and 50 mg/L of RC or MG concentration. Between each experiment, the photocatalyst was removed by filtration, then washed with distilled water at several times, and dried at 110°C for 12 h.

Results and discussion

XRD studies

Mineralogical analysis of the natural clay sample was identified by XRD measurements; evidenced the characteristic diffraction peaks of quartz (26.7), kaolinite (22.8) and illite (12.6) (Bel Hadjltaief et al. 2016). From the XRD spectrum of ZnO–Clay, shown in Figure 1, diffraction peaks appeared at 2θ equal to 31.8°, 34.4°, 36.2°, 47.5°, 55.6°, 62.8°, corresponding to hexagonal crystal lattices (100), (002), (101), (102), (110) and (103), respectively. ZnO presents the typical XRD diffraction pattern of wurtzite according to the standardized JCPDS Card No. 001-1136 (Li et al. 2014; Xu et al. 2015).

Based on the XRD results, the average crystal size of ZnO was calculated using the Debye–Scherrer equation as follows (Eq. (2)):

$$D = \frac{0.9\,\lambda}{\beta\cos(\theta)} \qquad (2)$$

where D is the crystallite size contribution to the peak width (integral or full width at half maximum) in radians, λ is wavelength of X-ray, β is full width at half maximum, and θ is the diffraction angle (Gnanaprakasam et al. 2015; Fatimah et al. 2011). The calculated average crystalline size of the ZnO on the clay obtained by Scherrer's equation was found to be around 13.65 nm (Table 1).

Textural analysis

Figure.2 shows the adsorption–desorption isotherms acquired for both the natural clay and the ZnO/clay photocatalyst. The specific surface area, pore radius and pore volume compared to natural clay are listed in Table 1. As expected, the specific area of the composite ZnO/Clay

material increased after ZnO deposition on the clay surface. The enhanced specific area suggests an increase in adsorption capacity for dyes molecules (Fatimah et al. 2011).

Fourier transform infrared spectroscopy studies

The infrared spectra of natural clay and ZnO/Clay are shown in Figure 3. The FTIR spectrum of raw clay shows bands at 3630 and 3440 cm^{-1} in the –OH stretching region; these two bands are assigned to the –OH stretching vibration of the structural hydroxyl groups in the clay and the water molecules present in the interlayer, respectively (Bel Hadjltaief et al. 2014). In addition, bands at 472 and 533 cm^{-1} can be assigned to Si-O-Mg and Si-O-Al, respectively (Bel Hadjltaief et al. 2014). In the FTIR spectra of ZnO–Clay sample, the bands at 3630 and 3440 cm^{-1} broaden due to the introduction of single bond OH groups: this is interpreted as impregnating effect in previous studies (Fatimah et al. 2011; Motshekga et al. 2013) dealing with the insertion of ZnO in Clay.

Electron microscopic analysis

The SEM micrographs of natural clay and ZnO/Clay are presented in Fig.4 . SEM images are fundamental to clarify the changes in the morphological features upon sol-gel ZnO deposition. Clearly, the surface morphology of natural clay (Fig. 4a) is different compared to ZnO/Clay sample (Fig. 4b). TEM images further confirm these changes in the morphology of the as prepared material (Fig. 5). It is notable from the TEM images that both nanoparticles ZnO adhere to the surface of clay, exhibiting good dispersion. The particle size in ZnO/Clay was found to range from 9 to 13.45 nm which in a good agreement with XRD results. The presence of ZnO was confirmed by energy dispersive X-ray spectroscopy (EDX). The EDX spectrum presented in Figure 5 indicates qualitatively the presence of Zn on the photocatalysts surface, also the

existence of certain elements, such as Si, Fe, Al, Mg, Ca, K, which are constituents of mineral composition of the natural clay. The ZnO content on the ZnO/Clay catalyst was found to be around 24 wt.%.

The adsorption of dye molecule onto catalyst surface is greatly influenced by pHpzc of catalyst, i.e. the pH at which the electrical charge density on catalyst surface is zero. At higher pH than pHpzc, catalyst surface is negatively charged and attracts cations. Conversely below pHpzc, catalyst surface is positively charged and repels cations (Bel Hadjltaief et al. 2016). Therefore, this parameter determines the ability of catalysts to adsorb either anionic or cationic dyes. The zero point charge of our ZnO/Clay photocatalyst was found to be 6.58.

Photocatalytic activity and mechanism of photodegradation

Figure 6 shows the measured of MG (pH 8) and RC (pH 3) removal efficiency as a function of reaction time, for the several experiments performed in the absence and in the presence of ZnO/Clay. The dyes did not undergo any decomposition under direct UV irradiation in the absence of ZnO/Clay. In the dark condition, absence UV irradiation, a maximal dyes conversion of discoloration amounting to 32.1% and 40.3% for RC and MG respectively. This initial conversion (32.08 and 40.25) is due to adsorption of both dyes on the catalyst surface. For the sake of comparison, the natural clay (prior to ZnO loading) was tested and only around 20–23% decolorization was obtained after 120 min of time on stream. The significant improvement of dye adsorption by ZnO/clay was related to the enhanced specific surface area from 36.6 m^2/g to 132.1 m^2/g. In the presence of UV irradiation, ZnO supported on natural clay is more active than commercial ZnO powder. It can be seen that the removal MG and RC using ZnO powder reached 78.9% and 63.6 % respectively within 120 min irradiation time. The enhanced

photocatalytic activity of ZnO/Clay can be attributed to the enhanced physicochemical properties of material, the highest concentration of active sites on ZnO/Clay and the highest specific surface area of ZnO/Clay compared to the raw natural clay and unsupported commercial ZnO.

Moreover, the photocatalytic activity of ZnO/Clay photocatalyst can be directly related to the holes induced through the release of electrons (e^-) from valance band to conduction band under UV light illumination (Zhou et al. 2015; Gnanaprakasam et al. 2015). Electron in the conduction band may reduce oxygen molecule to yield super oxide radical and holes generated in the conduction band may react with hydroxyl ions to form hydroxyl radicals. These radicals are strong oxidative agent leading to organic molecules conversion into CO_2 and H_2O molecules (Fig. 7).

The possible reaction scheme for the photocatalytic degradation of organic dyes from aqueous solution is given in Eqs. (3)–(7) (Bel Hadjltaief et al. 2014b; Zhou et al. 2015).

(i) photo-excitation with light of an energy greater than the ZnO band gap, which promotes the transfer of an electron, e , from the valence band to the conduction band, leaves an electronic vacancy or hole, h^+, in the valence band, and thus generates an electron–hole pair (Eq.3)

$$ZnO + h\nu \rightarrow h^+(VB) + e^-(CB) \quad (3)$$

(ii) Generation of reactive oxygen species such as $HO^\bullet$ and $O_2^{\bullet-}$ in the electron and hole are produced by H_2O and O_2 on the surface of ZnO (Eq.4–6)

$$h^+(VB) + H_2O \rightarrow HO^\bullet + H^+ \quad (4)$$

$$h^+(VB) + OH^- \rightarrow HO^\bullet + H^+ \quad (5)$$

$$e^-(VB) + O_2 \rightarrow O^-{}_2 \quad (6)$$

(iii) Attack of $HO^{\bullet}$ and $O_2^{\bullet-}$ to adsorbed dyes and their mineralization to CO_2 and H_2O and other degradation products through the various different paths (Eq.7)

$$HO^{\bullet} + \text{organic polluants} \rightarrow \text{intermidiates} \rightarrow CO_2 \uparrow + H_2O + \text{other degradation products} \quad (7)$$

Effect of operational parameters

In order to achieve efficient photocatalytic decolorization of RC and MG, the influence of the main operational parameters (initial pH, catalyst dosage, initial dye concentration, irradiation source and addition oxidizing agents) was evaluated.

Effect of pH

Wastewaters from textile industries usually have a wide range of pH values. Thus, pH can be one of the most important parameters for photodecolorization processes (Bel Hadjltaief et al. 2016) and it is therefore important to consider its influence on photocatalytic degradation of RC and MG. The effect of pH in range from 2 to 12 on the photodegradation of RC and MG was investigated under UV irradiation with initial dye concentration of 50 mg of ZnO/Clay. The obtained result was shown in Fig. 8. In case of MG, degradation efficiency increased with increase in pH >8 whereas, in case of RC, the higher degradation was observed in acid medium (pH<4). As mentioned before, the pHzpc of ZnO/clay was around 6.58. The surface charge is positive at pH value lower than pHzpc, neutral at pH and negative at higher pHzpc. The surface of photocatalyst is positively charged in acidic solutions and negatively charged in alkaline solution. As a result, the surface charge of the catalysts plays an important role in adsorption of positively charged MG molecules. Below pH_{pzc}, positively charged surface of catalysts caused repulsion for positively charged NH_2^+ (Dhiman et al. 2013). However, above pH_{pzc}, the

negatively charged surface of catalyst leads to higher adsorption of MG. While in case of CR, adsorption capacity of catalysts decreased with rise in pH from 2 to 12. In acidic solution (lower pH), there was increased protonation of CR. At pH > pH_{pzc}, adsorbent surface was negatively charged and repelled R-SO_3^- ions. The higher adsorption of CR at lower pH was apparently due to greater accessibility of CR to the active sites of adsorbents (Okte and Karamanis (2013)).

Effect of photocatalyst dosage

A series of experiments were carried out by varying the dosages of ZnO/Clay from 0.25 to 2 g L^{-1} in order to determine the effect of catalyst amounts. Color removal of RC or MG is depicted at different photocatalyst addition as shown in Figure 9. It can be seen that the percentage of removal of MG or RC is enhanced when the amount of catalyst in the reactor increases up to 0.8 g/L. However, up to this amount of catalyst the percentage of removal decreases slightly. The degradation efficiency enhancement in the presence a sufficient amount of catalyst in the solution is obviously due to the increase of the active material and thus ZnO active sites, resulting in enhanced free hydroxyl radical generation (Senthilvelan et al. 2013; Xu et al. 2015; Balcha et al. 2016). However, further increasing the catalyst dosage from 0.8 to 2.0 g/L resulted in a slight decrease in the decolorization efficiency, due to an increase in the turbidity of the suspension and a decrease in UV light penetration as a result of increased scattering effect (Muthirulan et al. 2013; Balcha et al. 2016).

Effect of initial dyes concentration

The decolorization of RC and MG were carried out at various initial concentrations ranging from 25 to 200 mg/L using ZnO/Clay dosage of 30 mg at initial pH of 8 (MG) and 3 (RC) under UV irradiation. It was found that the degradation ratio was inversely proportional to the initial

concentration of dyes. It can be seen in Fig. 10 that the removal percentage of dyes decreases exponentially with the increase in the initial concentration of dyes. The presumed reason is that when the initial concentration increases, more and more dye molecules are adsorbed on the surface of ZnO/Clay. Therefore, the generation of hydroxyl radicals will be reduced since there are only a fewer active sites for adsorption of hydroxyl ions and the generation of hydroxyl radicals. Further, as the concentration of a dye solution increases, the photons get intercepted before they can reach the catalyst surface, hence the absorption of photons by the catalyst decreases, and consequently the degradation percent is reduced. The present observations are also in agreement with results obtained by other groups of researchers (Muthirulan et al.2013; Ye et al. 2015; Bel Hadjltaief et al. 2016; Balcha et al. 2016).

Effect of inorganic anions

In textile industries, high concentrations of various inorganic salts such as Chloride (Cl^-), carbonate (HCO_3^-), sulfate (SO_4^{2-}) and Nitrate (NO_3^-) are frequently used to improve the dyeing rate of dyes. Some studies examined the impact of inorganic ions on the photocatalytic decolorization of organic pollutants (Yajun et al. 2013; Wang et al. 2015, Borthakur et al. 2016 Dugandži et al. 2017). For example Niu and Hao have investigated the influence of the inorganic salts and surfactants on the degradation of organic dye using titanium dioxide–silicotungstic acid nanocomposite films and concluded that the presence of NaCl and Na_2SO_4 inhibit the degradation efficiency of the photocatalyst (Niu and Hao. 2014). To examine the anion effect, the influence of several anions (Cl^-, HCO_3^-, SO_4^{2-} and NO_3^-) on the reaction rate of RC and MG was examined. In this study, the effect of different anions were studied by adding 8 mL of sodium salt (1×10^{-3} mol/L) of Cl^-, HCO_3^-, SO_4^{2-} and NO_3^- ions separately to 50 mg/L of RC or MG dye solution with catalyst loading of 300 mg/L at pH 5 (normal pH of the medium

containing catalyst). The Results are shown in Fig. 11. It can be observed that the presence of the all anions inhibits the photocatalytic activity following the order of Cl^- > HCO_3^- > NO_3^- > SO_4^{2-}. This can be explained on the basis of reaction of h_{VB}^+ and $HO^\bullet$ with anions that behave as scavengers, thus inhibiting the degradation of organic molecules (Yajun et al. 2013; Wang et al. 2015, Borthakur et al. 2016; Dugandži et al. 2017), according to reactions (8)–(11):

$$HCO_3^- + HO^\bullet \rightarrow CO_3^{-\bullet} + H_2O \quad (8)$$

$$NO_3^- + HO^\bullet \rightarrow NO_3^{\bullet-} + OH^- \quad (9)$$

$$Cl^- + HO^\bullet \rightarrow Cl^\bullet + OH^- \quad (10)$$

$$SO_4^{2-} + H_2O \rightarrow SO_4^{2-} + HO^\bullet + H^+ \quad (11)$$

Effect of irradiation source and kinetics of photodecolorization

The effect of irradiation time on decolorization efficiency of RC and MG was studied by keeping the optimal parameters obtained above (MG: pH= 8, $[MG]_0$=50mg/L, $[catalyst]_0$ =1g/L) and RC; pH=3, $[RC]_0$=50mg/L, $[catalyst]_0$ =0.8g/L). During these photodegradation experiments, samples were irradiated with solar light and a 100 W UV lamp separately, in order to prove effectiveness of Solar and UV irradiation sources. The results presented in Fig.12 shows that the degradation of the RC and MG is possible under both irradiation sources. The decolorization efficiency in the presence of UV irradiation was however lower than under solar light. Similar results were found by Han and co-workers, who reported that solar irradiation was found to be highly effective solar than UV irradiation for estrone photocatalytic degradation using either ZnO or P25 TiO_2 (Han et al. 2012). Not surprisingly, we can notice that oxidation of RC, a diazo dye, is more difficult in comparison to MG due to its lower molecular weight and less complex

chemical structure (Bel Hadjltaief et al. 2013). In addition, the mineralization of RC and MG was measured using COD removal efficiency. The results show that COD removal efficiency reached 88.6 and 90.6% for RC and MG respectively during 180 min of irradiation treatment.

The kinetics of RC and MG decolorization by ZnO/Clay photocatalyst are analyzed using the first-order model expressed in Eq (12).

$$\ln\left(\frac{C_0}{C_t}\right) = k_{app} \times t \qquad (12)$$

In which k_{app} is the apparent rate constant of the first-order reaction (min^{-1}), C_0 and Ct are the concentrations (mg/L) of the RC or MG dye at time 0 and t, respectively. A plot of ln (C_0/C_t) versus time represents a straight line; the slope equals the apparent first order rate constant k_{app}. Table 2 lists the apparent first-order rate constants (k_{app}) using ZnO/Clay photocatalyst under both irradiation sources, which were calculated from Figure 12. For both irradiation sources, the rates of photocatalytic activity of MG was higher than RC (Table 2). ~~In this sense, the bigger and more sluggish molecules of RC will more difficultly reach the catalytic active sites situated in the inner porosity of the ZnO/Clay material.~~

Reusing of the Photocatalytic Material

Reusability study is an integral part of any catalytic investigation of any photocatalysts. Reminding in view the importance of this study, we performed the photocatalytic experiment to determine the extent of reusability of the catalyst. The reusability of ZnO/Clay photocatalyst was studied at optimum condition pH 8 for MG and pH 3 for RC, 0.8 g/L catalyst and 50 mg/L of RC or MG concentration. The reusability of ZnO/Clay was investigated efficiently up to five cycles and the results are given in Figure 13. After each cycles, the photocatalyst was distilled water several times, and dried at 110 °C for 12 h. No significant change in the activity of the catalyst

was observed up to 4th cycle. However, the catalyst tends to lose its activity from cycle 5rd. in this case, the decolorization percentage of RC and MG reached 98.1% and 96.9% respectively by ZnO/Clay. These results implied that the ZnO/clay possessed higher recyclability. Based on the above results, it indicates a possibility for application of ZnO supported natural Tunisian clay photocatalyst in the wastewater treatment.

Comparison of degradation percentages of CR and MG dyes with available literature

A comparison between the present study and studies conducted by researchers regarding the photodegradation of CR and MG is shown in Table 3. This comparative study proved the effectiveness of the synthesized ZnO/Clay as a photocatalyst over others metal oxide based catalysts reported in the literature. As it can be seen, the obtained maximum CR and MG decolorization by prepared ZnO supported natural Tunisian Clay was more favorable than those of other catalysts. The high efficiency of our system was related to the choice of preparation method and the nature of catalytic support.

Conclusion

A ZnO/Clay composite, i.e. ZnO immobilized on Tunisian clay, was prepared by sol-gel method and characterized in order to gain more insight about its structure, morphology and physico-chemical properties. The XRD patterns evidenced the presence of ZnO clusters at small sizes, i.e. from 9 to 15 nm, pointing to its high disperson on the clay surface. The presence of ZnO was further confirmed by TEM, SEM and FTIR analyses. The ZnO/Clay composite was used in the the photocatalytic degradation of Red Congo and Malachite Green in aqueous solutions. The photocatalytic reaction was found to be sensitive to several operational parameters, such as pH of the solution, catalyst dosage, concentration of the dyes, irradiation source, and the presence of

inorganic ions. The results showed that both dyes could be effectively removed from the aqueous media by means a heterogeneous photocatalytic process in the presence of ZnO/Clay, even in the presence of solar irradiation, thus demonstrating the feasibility of using this particular Tunisian clay in the present application.

ACKNOWLEDGMENTS

The authors thank the University of Sfax and UPMC Sorbonne University for allowing access to their respective technical facilities.

References

Abedi K, Ghorbani SF, Jaleh B, Bahrami A, Yarahmadi R, Haddadi R, Gandomi M (2015) Decomposition of chlorinated volatile organic compounds (CVOCs) using NTP coupled with TiO_2/GAC, ZnO/GAC, and TiO_2-ZnO/GAC in a plasma-assisted catalysis system. J Electrostatics 73:80-88

Alexandre GS, Prado, Leonardo L. Costa (2009) Photocatalytic decouloration of malachite green dye by application of TiO_2 nanotubes. J Hazard Mat 169:297–301 Balan E, Saitta AM, Mauri F, Calas G, (2001) First principles modeling of the infrared spectrum of kaolinite, American Mineralogist 86:1321–1330

Balcha A, Yadav OP, Dey T (2016) Photocatalytic degradation of methylene blue dye by zinc oxide nanoparticles obtained from precipitation and sol-gel methods. Environ Sci Pollut Res 23:25485–25493. doi: 10.1007/s11356-016-7750-6

Bel Hadjltaief H, Ben Zina M, Galvez ME, Da Costa P (2016) Photocatalytic degradation of methyl green dye in aqueous solution over natural clay-supported ZnO–TiO2 catalysts. J

Photochem Photobiol A Chem 315:25–33. doi: 10.1016/j.jphotochem.2015.09.008

Bel Hadjltaief H, Da Costa P, Beaunier P, et al (2014a) Fe-clay-plate as a heterogeneous catalyst in photo-Fenton oxidation of phenol as probe molecule for water treatment. Appl Clay Sci 91–92:46–54. doi: 10.1016/j.clay.2014.01.020

Bel Hadjltaief H, Da Costa P, Elena Galvez M, Ben Zina M (2013) Influence of Operational Parameters in the Heterogeneous Photo- Fenton 435 Discoloration of Wastewaters in the Presence of an Iron- Pillared Clay. Ind Eng Chem Res 52:16656−16665. doi: 10.1021/ie4018258

Bel Hadjltaief H, Sdiri A, Ltaief W, Da Costa P, Elena Galvez M, Ben Zina M (2017) Efficient removal of cadmium and 2-chlorophenol in aqueous systems by natural clay: Adsorption and photo-Fenton degradation processes. C. R. Chimie 1−10.doi.org/10.1016/j.crci.2017.01.009.

Bel Hadjltaief H, Galvez ME, Ben Zina M, Da Costa P (2014b) TiO2/clay as a heterogeneous catalyst in photocatalytic/photochemical oxidation of anionic reactive blue 19. Arab J Chem. doi: 10.1016/j.arabjc.2014.11.006

Borthakur P, Boruah PK, Darabdhara G, Sengupta P, Das MR, Boroninc AI, Kibis LS, Kozlova MN, Fedorov V E (2016) Microwave assisted synthesis of CuS-reduced graphene oxide nanocomposite with efficient photocatalytic activity towards azo dye degradation. J Environ Chem Eng http://dx.doi.org/10.1016/j.jece.2016.10.023

Bouzid J, Elouear Z, Ksibi M, Feki M, Montiel A (2008) A study on removal characteristics of copper from aqueous solution by sewage sludge and pomace ashes. J Hazard Mater 152:838–845

Dhakshinamoorthy A, Visuvamithiran P, Tharmaraj 454 V, Pitchumani K (2011) Clay encapsulated ZnO nanoparticles as efficient catalysts for N-benzylation of amines.Catal Com

16:15–19

Dhiman P, Chand J, Kumar A, Kotnala RK, Batoo KM, Singh M (2013) Synthesis and characterization of novel Fe@ZnO nanosystem . J Alloys Compd 578:235–241

Dugandži A M, Tomaševi A V, Radiši MM, Šekuljica N Ž, Mijin D Ž,. Petrovi S D (2017) Effect of inorganic ions, photosensitisers and scavengers on the photocatalytic degradation of nicosulfuron. J Photochem Photobiol A: Chem 336 146–155

Fatimah I, Wang S, Wulandari 456 D (2011) ZnO/montmorillonite for photocatalytic and photochemical degradation of methylene blue. App Clay Sci 53:553–560

Forgacs E, Cserháti T, Oros G (2004) Removal of synthetic dyes from wastewaters: a review. Environ Int 30:953–971. doi: 10.1016/j.envint.2004.02.001

Gnanaprakasam A, Sivakumar VM, Sivayogavalli PL, Thirumarimurugan M (2015) Characterization of TiO_2 and ZnO nanoparticles and their applications in photocatalytic degradation of azodyes. Ecotoxicol Environ Saf 121:121–125. doi:10.1016/j.ecoenv.2015.04.043

Han J, Liu Y, Singhal N, Wang L, Gao W (2012) Comparative photocatalytic degradation of estrone in water by ZnO and TiO_2 under artificial UVA and solar irradiation. Chem Eng J 213:150–162

Li SQ, Zhou PJ, Zhang WS, Chen S, Peng H (2014) Effective photocatalytic decolorization of methylene blue utilizing ZnO/rectorite nanocomposite under simulated solar irradiation. J Alloys and Comp 616:227–234

Muthirulan P, Meenakshisundararam M, Kannan N. (2013) Beneficial role of ZnO photocatalyst supported with porous activated carbon for the mineralization of alizarin cyanin green dye in

458 aqueous solution. J Advanced Res 4:479–484

459 Motshekga SC, Raya SS, Onyango MSM, Momba NB (2013) Microwave assisted synthesis,
460 characterization and antibacterial activity of Ag/ZnO nanoparticles supported bentonite clay. J
461 Hazard Mat 262:439–446

462 Nezamzadeh-Ejhieh A, Khorsandi S (2014) Photocatalytic degradation of 4-nitrophenol with
463 ZnO supported nano-clinoptilolite 477 zeolite. J Ind Eng Chem 20:937-946

464 Niua P, Hao J (2014) Efficient degradation of organic dyes by titanium dioxide–silicotungstic
465 acid nanocomposite films: Influence of inorganic salts and surfactants Colloids and Surfaces A:
466 Physicochem. Eng. Aspects 443:501–507

467 Okte AN, Karamanis D, (2013) Anovel photoresponsive ZnO-flyash nanocomposite for
468 environmental and energy applications. Appl Catal B 142–143:538–552

469 Ong CB, Mohammad AW, Rohani R, et al (2016) Solar photocatalytic degradation of hazardous
470 Congo red using low-temperature synthesis of zinc oxide nanoparticles. Process Saf Environ
471 Prot 104:549–557. doi: 10.1016/j.psep.2016.04.006

472 Pradhan G K, Reddy KH, Parida KM (2014) Facile fabrication of mesoporous -Fe2O3/SnO2
473 nanoheterostructure for photocatalytic degradation of malachite green. Catalysis Today 224:171–
474 179

475 Reddy CV, Shim J, Cho M (2017) Synthesis, structural, optical and photocatalytic properties of
476 CdS/ZnS core/shell nanoparticles. J Phys Chem Solids 103:209–217. doi:
477 10.1016/j.jpcs.2016.12.011

478 Saikia L, Bhuyan D, Saikia M, et al (2015) Photocatalytic performance of ZnO nanomaterials for

self sensitized degradation of malachite green dye under solar light. Appl Catal A Gen 490:42–49. doi: 10.1016/j.apcata.2014.10.053

Seyghali, B., M. A. Zanjanch (2015) Photocatalytic activity of TiO2 nanoparticles synthesized in presence of ammonium hexafluorosilicate. Spectro. Acta Part A: Mol. Biomol. Spect. 151,104–110.

Senthilvelan S, Chandraboss VL, Karthikeyan B, Natanapatham 498 L, Murugavelu M (2013) TiO_2,ZnO and nanobimetallic silica catalyzed photodegradation of methylgreen. Mater. Sci. Semicond Process 16:185–192

Soltani D, Rezaee CR, Khataee A, Safari M (2014) Photocatalytic process by immobilized carbon black/ZnO nanocomposite for dye removal from aqueous medium: Optimization by response surface methodology. J Ind Eng Chem 20:1861–1868

Wei, S., X. Hu, H. Liu, Q. Wang, C. He (2015) Rapid degradation of Congo red by molecularly imprinted polypyrrole-coated magnetic TiO2 nanoparticles in dark at ambient conditions. J. Hazard. Mater. 294, 168–176.

Xu H, Yu T, Liu J (2014) Photo-degradation of Acid Yellow 11 in aqueous on nano-ZnO/Bentonite under ultraviolet and visible light irradiation. Mat Letters, 117: 263–265

Xu H, Zhang D, Xu A, Wu F, Cao R. (2015) Quantum Sized Zinc Oxide Immobilized on Bentonite Clay and Degradation of C.I. Acid Red 35 in Aqueous under Ultraviolet Light. Internat J Photoenergy 2015: 7–17

Ye J, Li X, Hong J, Chen J, Fan Q (2015) Photocatalytic degradation of phenol over ZnO nanosheets immobilized on montmorillonite. Mat Sci in Semic Pro 39: 17–22

Yajun W, Kecheng L, Changgen F (2013) Influence of inorganic anions and organic additives on photocatalytic degradation of methyl orange with supported polyoxometalates as photocatalyst. J of Rare Earths, 31:360–365

Zhou Y, Liu F, Yu S (2015) Preparation and photo-catalytic activities of FeOOH/ZnO/MMT composite. Appl Sur Sci 355:861–867

Figures caption

Fig.1. XRD patterns of Raw Clay and ZnO/Clay (b) samples.

Fig.2. N_2 adsorption isotherms of Raw Clay and ZnO/Clay (b) samples.

Fig.3. FTIR spectra for Raw Clay (a) and ZnO/Clay (b) samples.

Fig.4. SEM images of Raw Clay (a) and ZnO/Clay (b) samples.

Fig. 5.TEM images and EDS spectra for Raw Clay and ZnO/Clay

Fig.6. Decolorization efficiency as a function of reaction time, under different catalytic systems and reaction conditions for (a) MG and (b) RC (initial dyes concentration= 50mg L^{-1}, photocatalyst amount = 1 gL^{-1}, pH 8 for MG and pH 3 for RC and T = 25°C).

Fig.7. Mechanism of photocatalytic degradation of organic dyes.

Fig. 8. Effect of pH on photocatalytic decolorization of dyes using ZnO/Clay (initial dyes concentration= 50mg L^{-1}, photocatalyst amount = 1gL^{-1} and T = 25°C).

Fig. 9. Effect of catalyst loading on photocatalytic decolorization of dyes using ZnO/Clay (initial dyes concentration= 50mg L^{-1}, pH 6.32 for MG and pH 6.32 for RC and T = 25°C).

Fig. 10. Effect of concentration on photocatalytic decolorization of dyes using ZnO/Clay (photocatalyst amount = 1gL^{-1}, pH 6.32 for MG and pH 6.32 for RC and T = 25°C).

Fig. 11. Effect of different anions on photocatalytic decolorization of (a) MG and (b) RC (initial dyes concentration= 50mg L^{-1} , photocatalyst amount = 1gL^{-1}, pH 6.32 for MG and pH 6.32 for RC and T = 25°C).

Fig.12. Effect of irradiation time on photocatalytic decolorization of dyes (initial dyes concentration= 50mg L^{-1}, photocatalyst amount = 1gL^{-1}, pH 6.32 for MG and pH 6.32 for RC and T = 25°C).

Fig. 13. Decolorization efficiency through three consecutive photocatalysts reuse cycles.

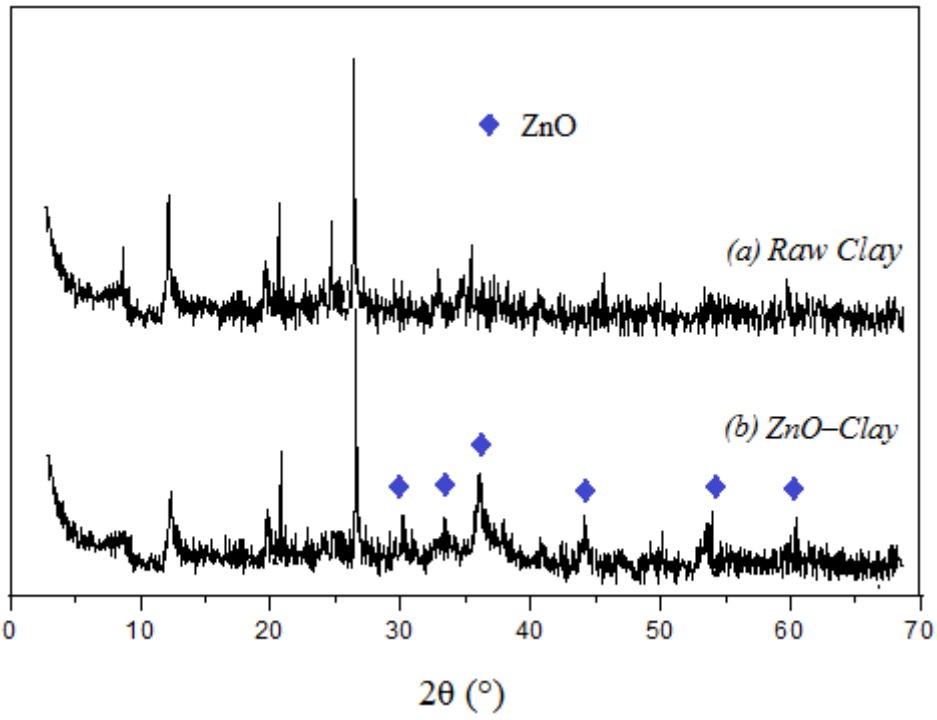

Fig. 1. XRD patterns of Raw Clay and ZnO/Clay (b) samples

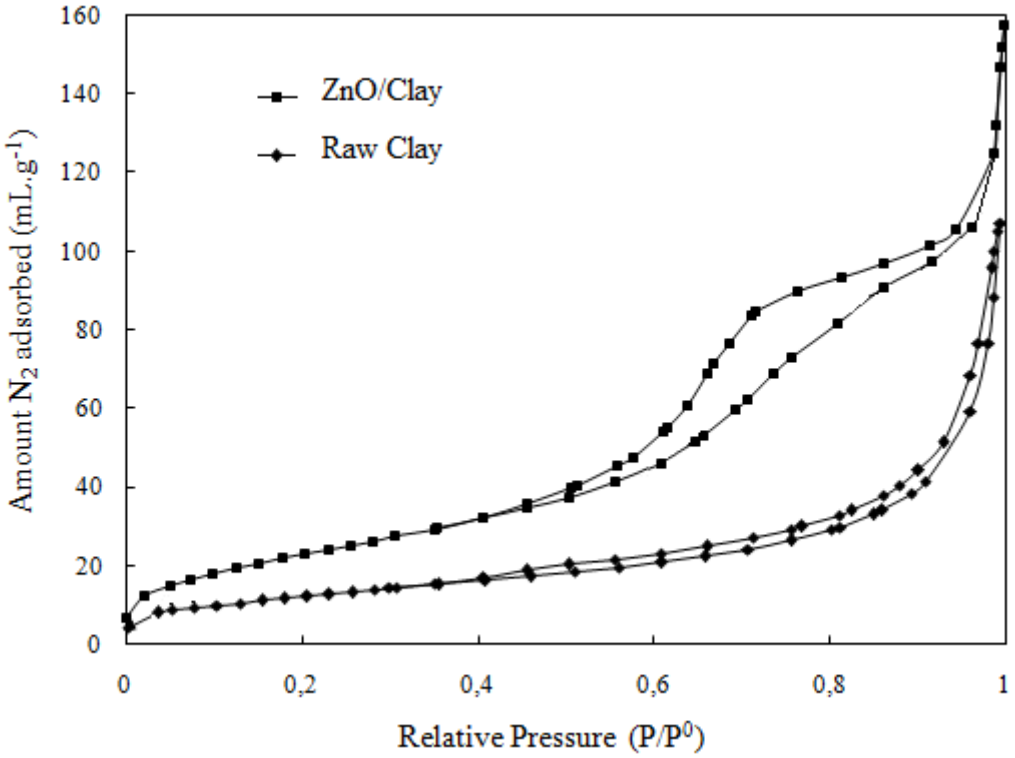

Fig. 2. N_2 adsorption isotherms of Raw Clay and ZnO/Clay (b) samples

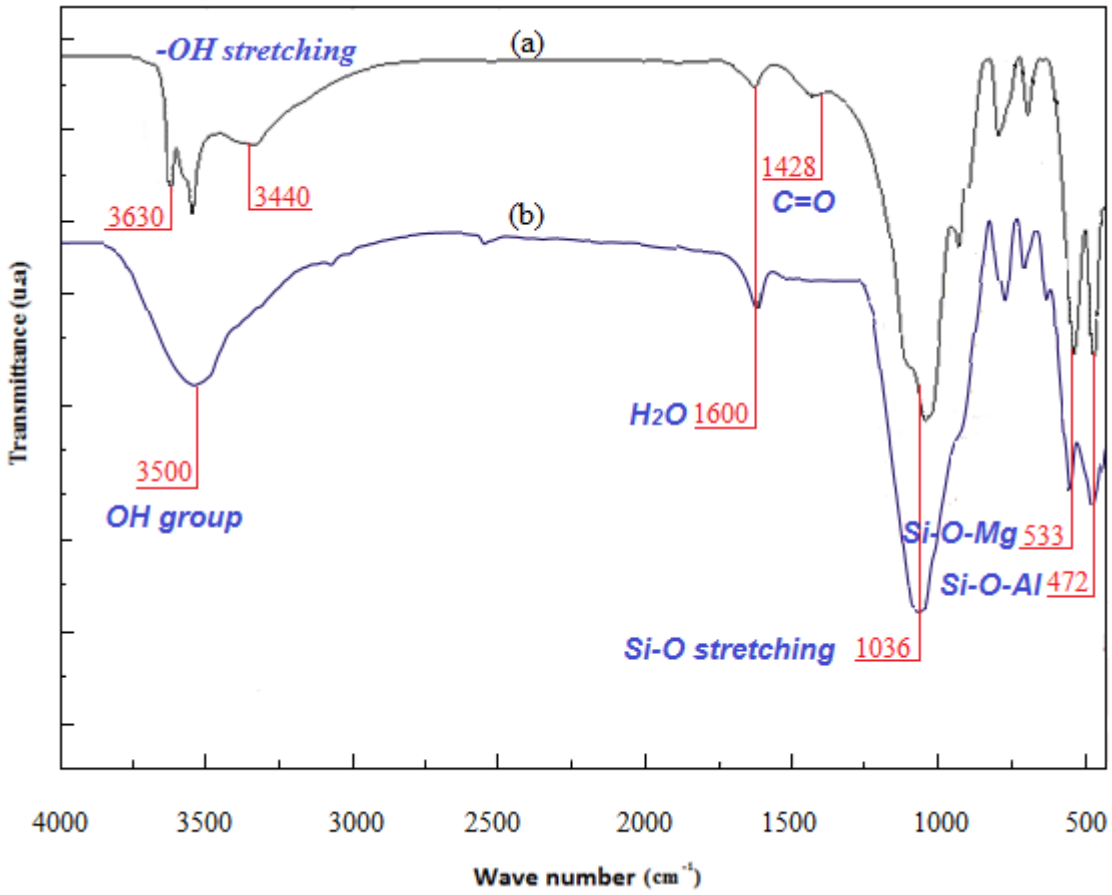

Fig.3. FTIR spectra for Raw Clay (a) and ZnO/Clay (b) samples.

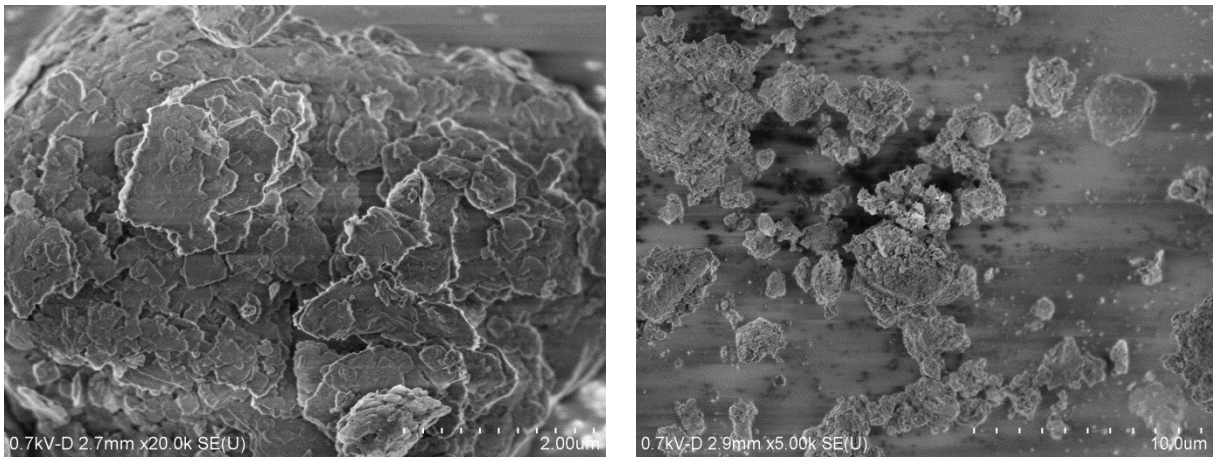

(a) Raw Clay (b) ZnO/Clay

Fig.4. SEM images of Raw Clay (a) and ZnO/Clay (b) samples

Natural clay

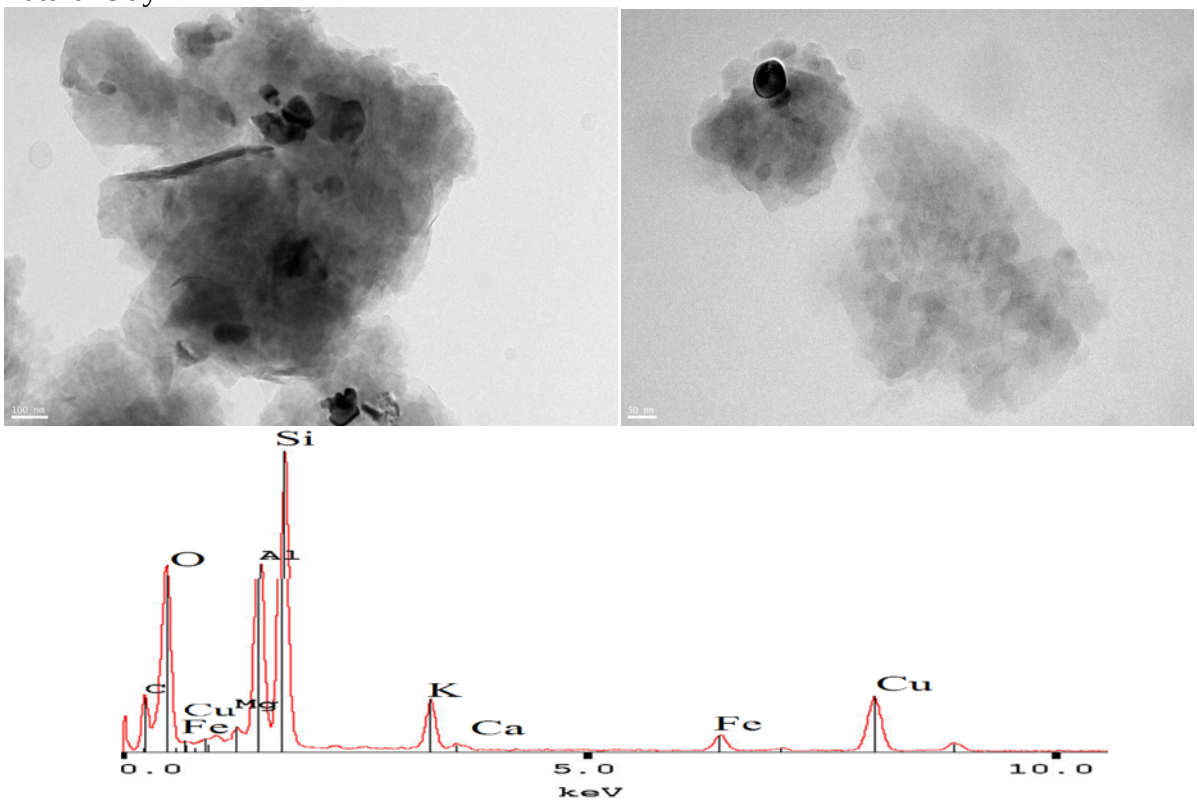

ZnO/Clay

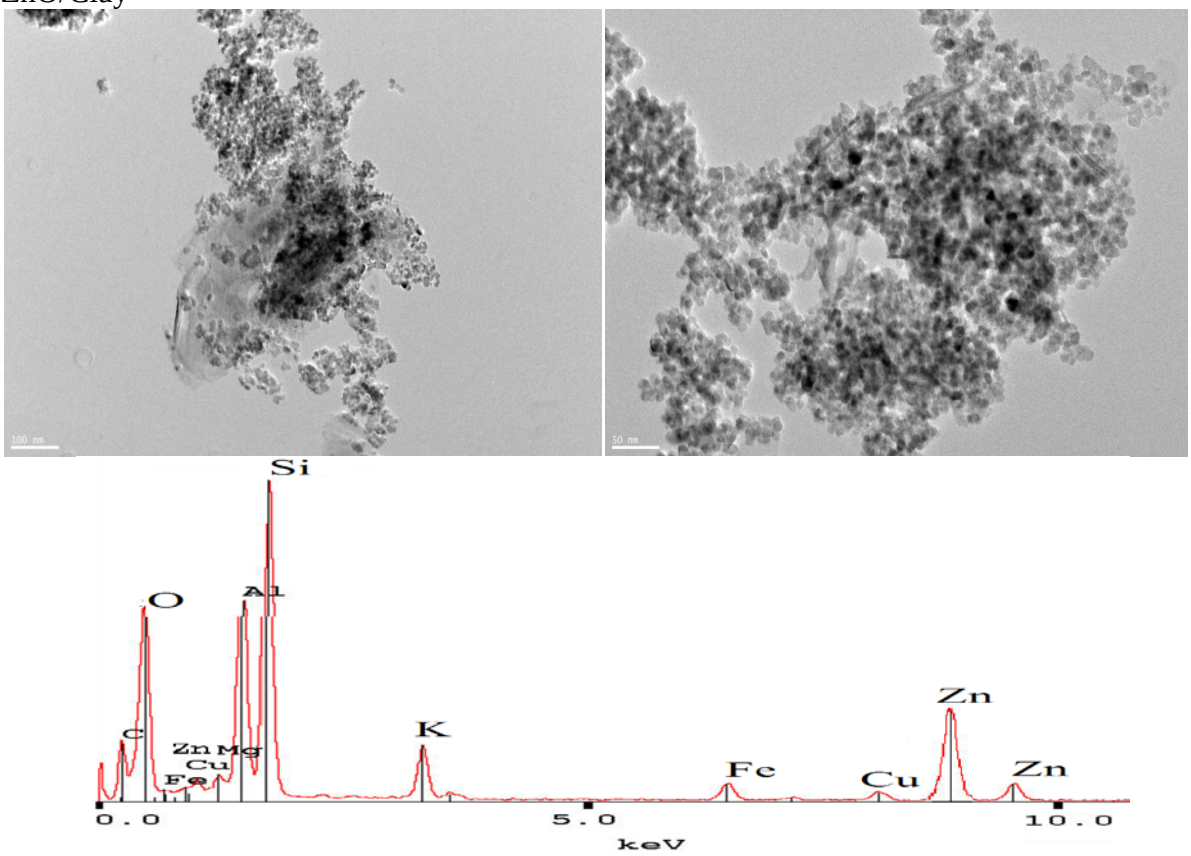

Fig. 5. TEM images and EDS spectra for Raw Clay and ZnO/Clay

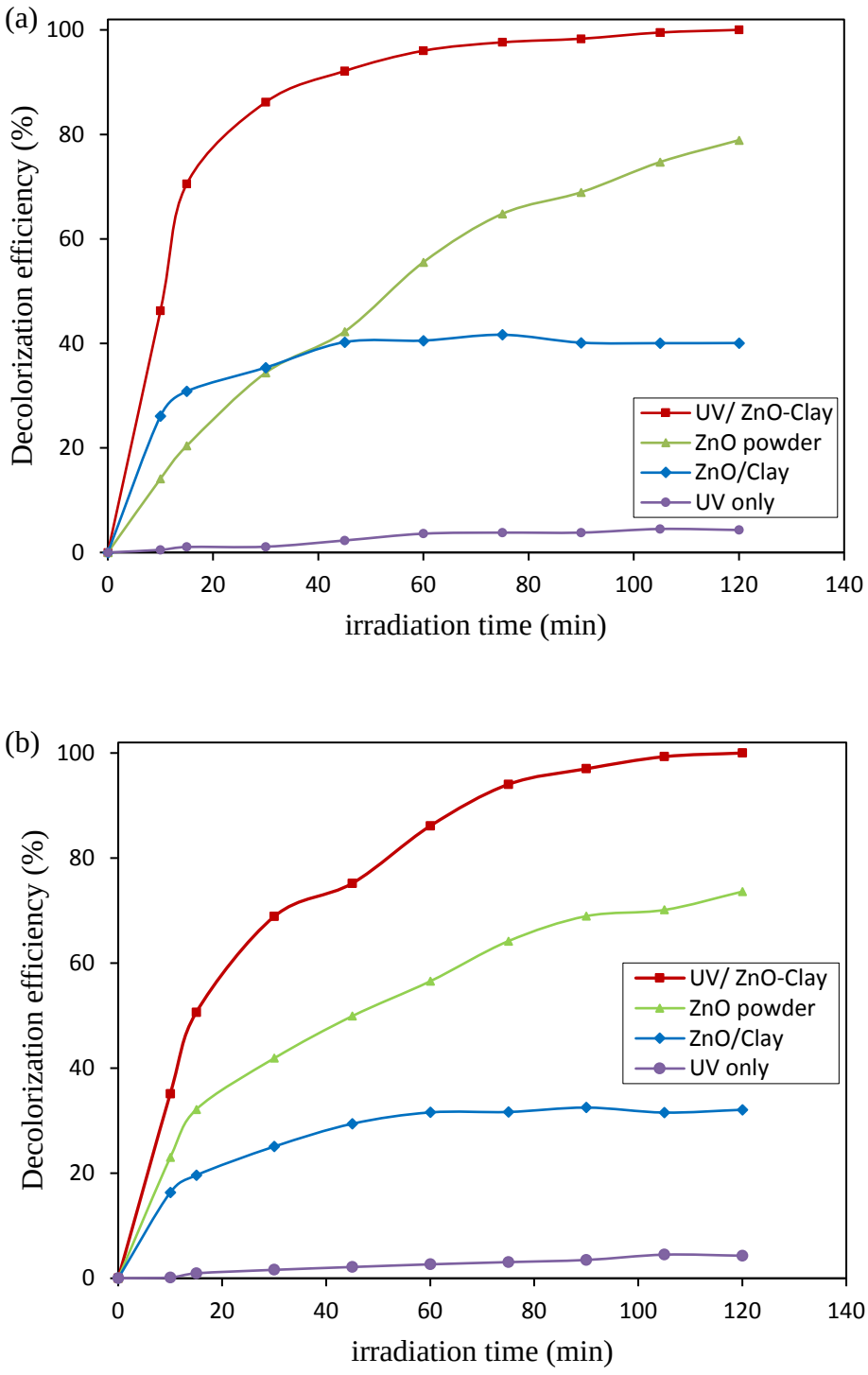

Fig.6. Decolorization efficiency as a function of reaction time, under different catalytic systems and reaction conditions for (a) MG and (b) RC (initial dyes concentration= 50mg L^{-1}, photocatalyst amount = 1 gL^{-1}, pH 8 for MG and pH 3 for RC and T = 25°C).

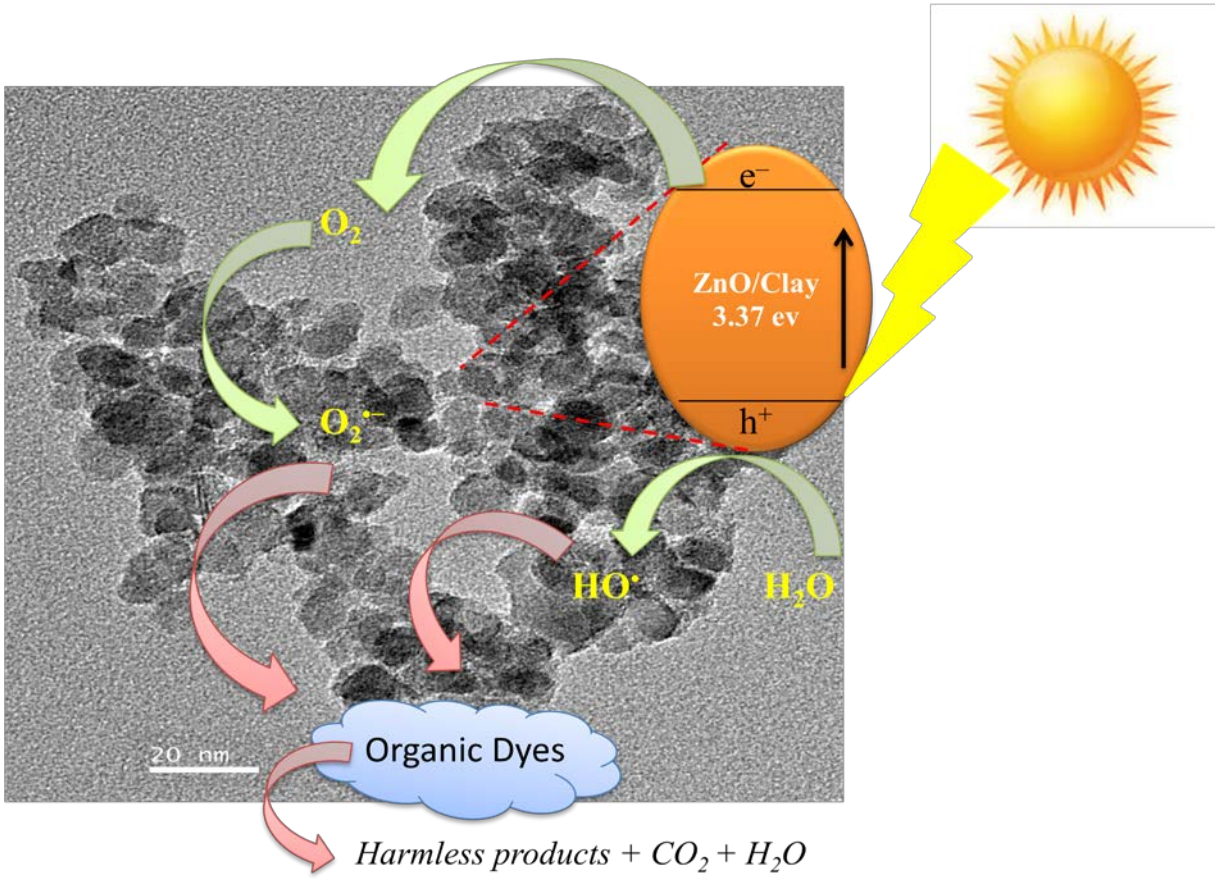

Fig. 7. Mechanism of photocatalytic degradation of organic dyes

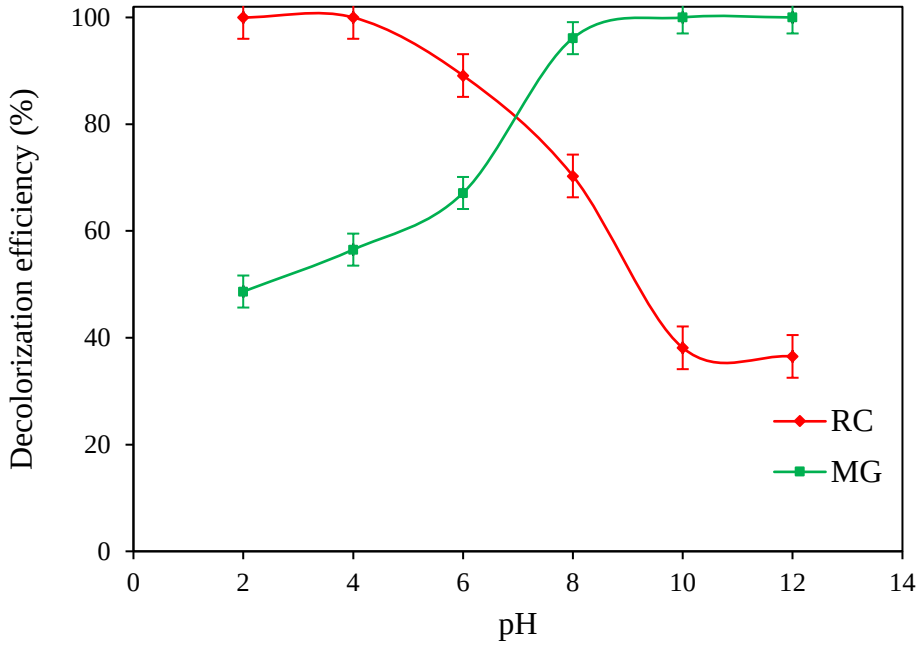

Fig. 8. Effect of pH on photocatalytic decolorization of dyes using ZnO/Clay (initial dyes concentration= 50mg L^{-1}, photocatalyst amount = 1gL^{-1} and T = 25°C).

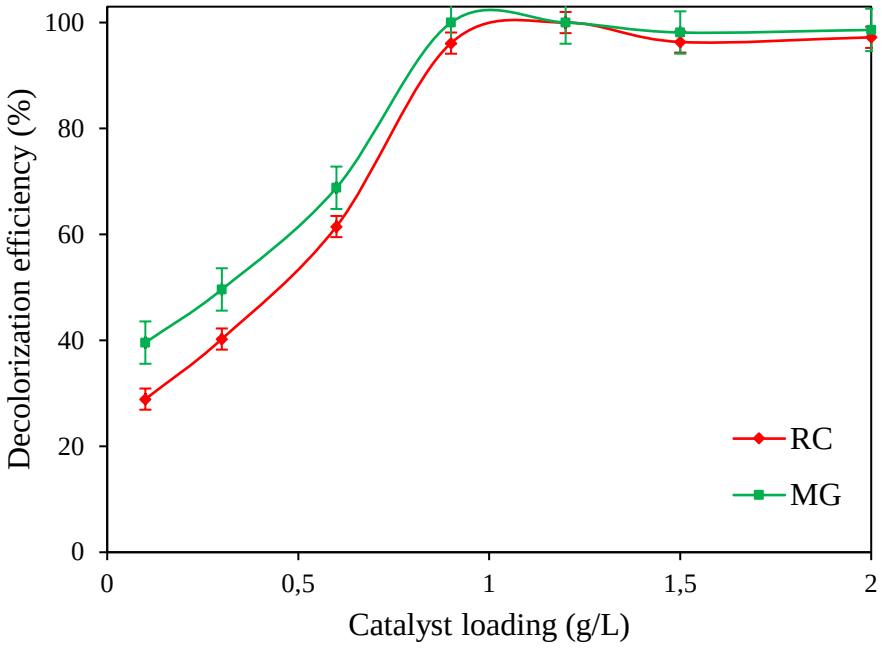

Fig.9. Effect of catalyst loading on photocatalytic decolorization of dyes using ZnO/Clay (initial dyes concentration= 50mg L^{-1}, pH=8 for MG and pH=3 for RC and T = 25°C).

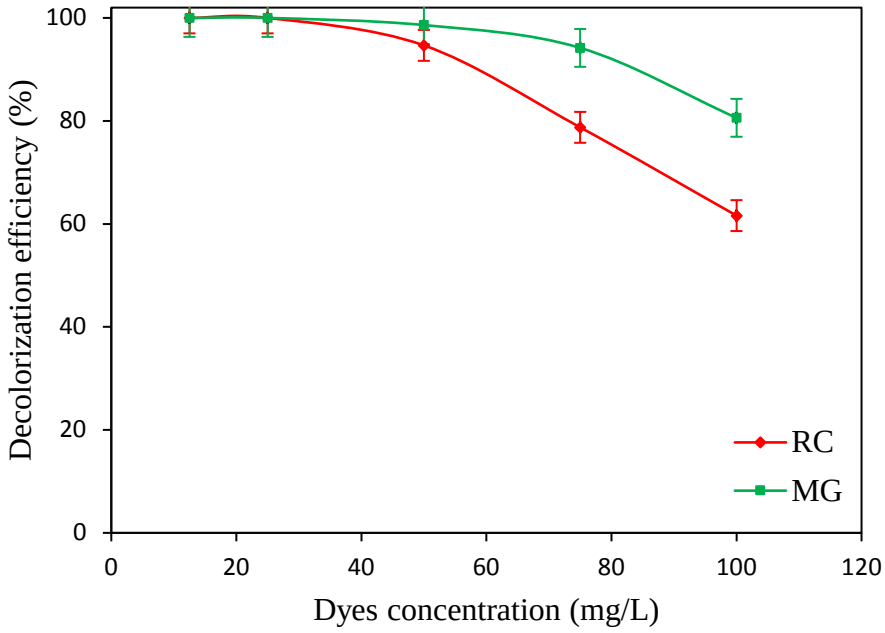

Fig.10. Effect of concentration on photocatalytic decolorization of dyes using ZnO/Clay (photocatalyst amount = $1gL^{-1}$, pH 8for MG and pH 3 for RC and T = 25°C).

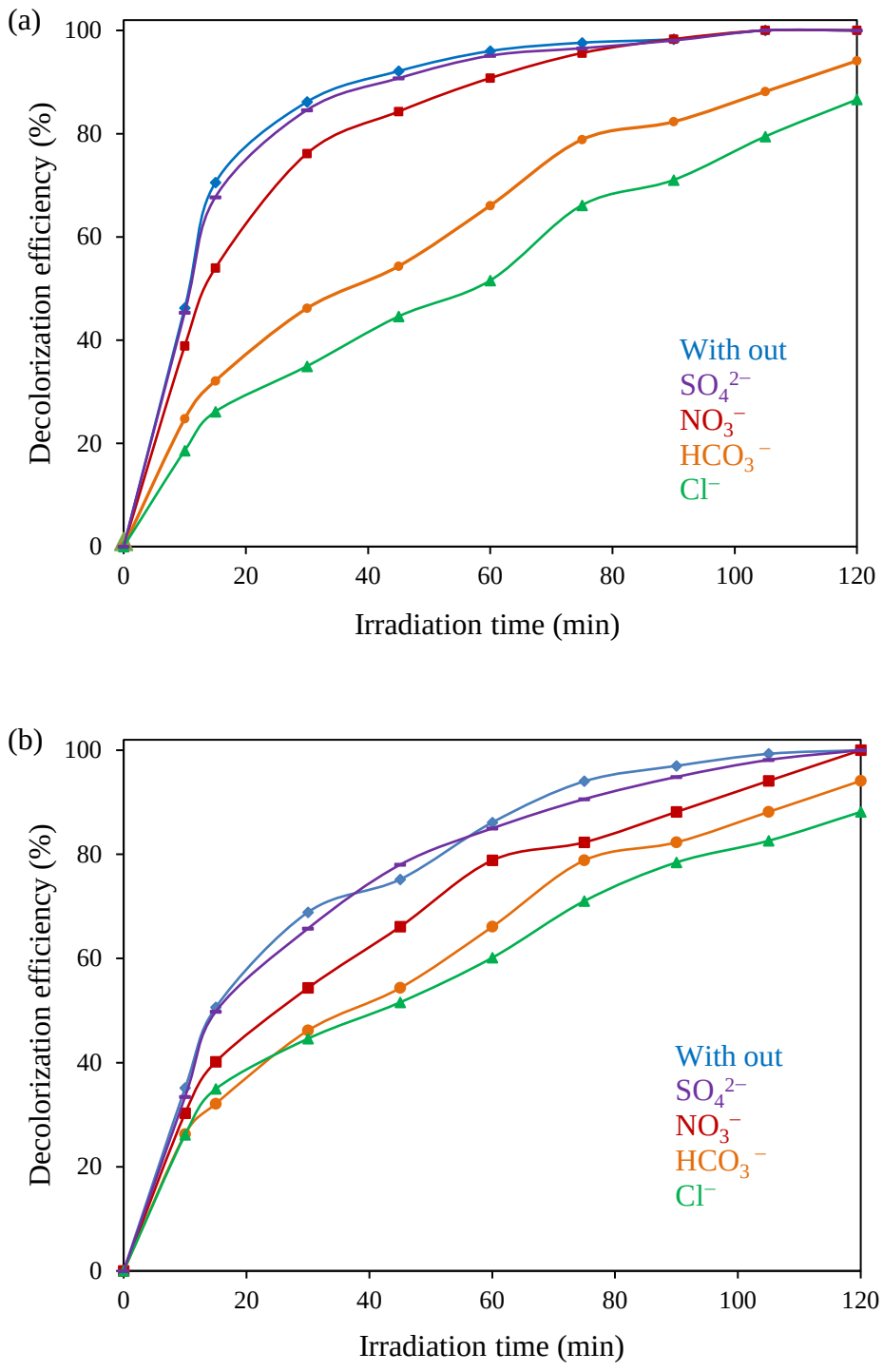

Fig.11. Effect of different anions on photocatalytic decolorization of (a) MG and (b) RC (initial dyes concentration= 50 mg L^{-1}, photocatalyst amount = 1gL^{-1}, pH 8 for MG and pH 3 for RC and T = 25°C).

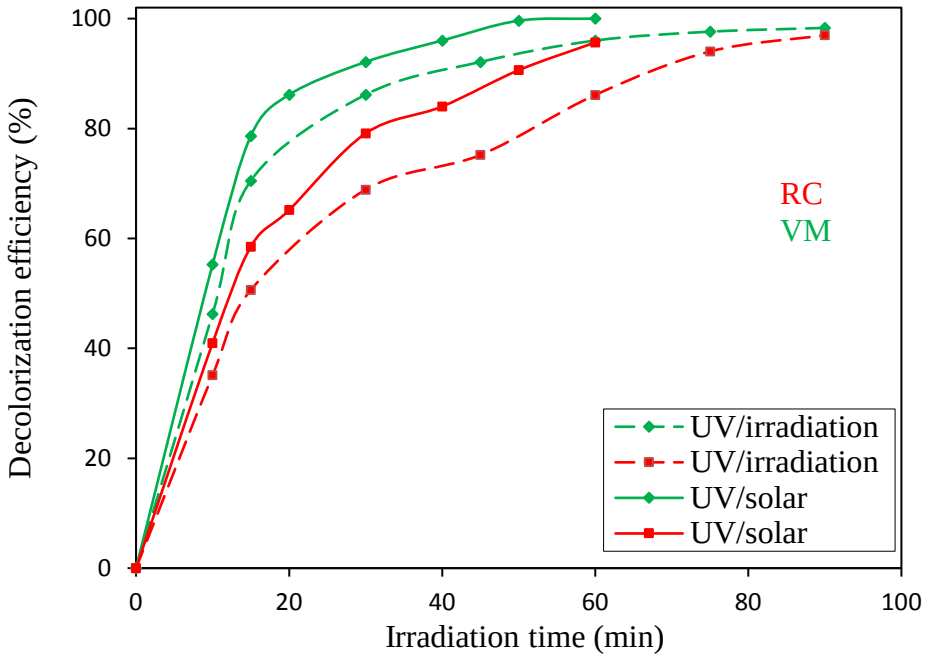

Fig.12. Effect of irradiation time on photocatalytic decolorization of dyes (initial dyes concentration= 50mg L^{-1}, photocatalyst amount = 1gL^{-1}, pH 8 for MG and pH 3 for RC and T = 25°C).

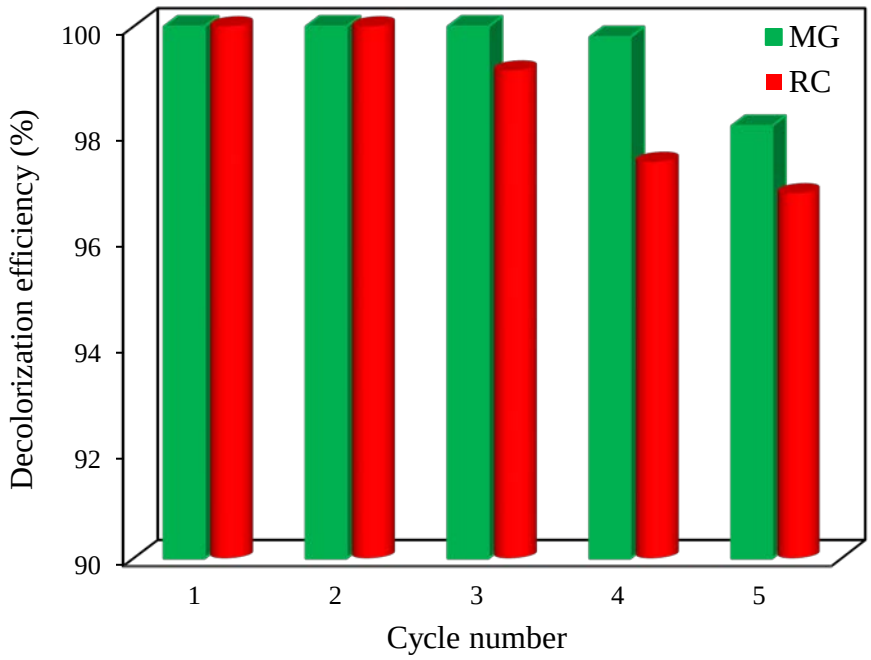

Fig. 13. Decolorization efficiency through three consecutive photocatalysts reuse cycles.

Tables

Table 1: Textural and structural properties of the samples.

	Sample	
	Raw Clay	ZnO/Clay
S_{BET} (m^2/g)	36.7	132.1
Total pore volume (cm^3/g)	0.132	0.255
Pore diameter (nm)	2.24	5.68
Crystallite size, D (nm)	n.d	13.65
ZnO content (wt %)	n.d	24.35

Table 2: Pseudo-First-Order Kinetic Parameters for Discoloration of RC and MG in the presence of photocatalyst under UV and solar irradiation.

	UV irradiation		Solar irradiation	
	K_{app}	R^2	K_{app}	R^2
MG	0.033	0.9844	0.0219	0.9701
RC	0.0238	0.9808	0.0146	0.98

Table 3 Comparison of degradation percentages of MG and RC dyes with literature.

dye	Catalyst	method	Source of irradiation	Highest degradation (%), time	Ref.
MG	ZnO	hydrothermal	solar radiation	83.68, 100	Saikia et al. 2015
	TiO2	hydrothermal	125W Hg lamp	100; 105 min	Alexandre et al. 2009
	Fe_2O_3/SnO_2	coprecipitation	solar radiation	86, 360 min	Pradhan et al. 2014
	ZnO/Clay	sol–gel	100 W lamp	97.18, 60 min	In this work
			solar radiation	100, 60 min	
RC	ZnO	sol–gel	Solar light	94.5, 60 min	Ong et al. 2016
	TiO_2	sol–gel	400WKr lamp	98, 80 min	Seyhali et al. 2015
	Fe_3O_4-TiO_2	coated magnetic	UV+ Microwave	93, 300 min	Wei et al. 2015
	ZnO/Clay	sol–gel	100 W lamp	100, 70 min	In this work
			solar radiation	97, 90 min	